Journal of Physics: Conference Series **415** (2013) 012035 doi:10.1088/1742-6596/415/1/012035

Are stereograms holograms? A human perception analysis of sampled perspective holography

Pierre St. Hilaire, Pierre-Alexandre Blanche, Cory Christenson, Ram Voorakaranam, Lloyd LaComb, Brittany Lynn, Nasser Peyghambarian

College of Optical Sciences, The University of Arizona, Tucson, Arizona 85721, USA

philaire@optics.arizona.edu

Abstract. In this paper, we analyze the optical performance of a commonly used 1-step recording geometry for stereograms and compare it to the fully fringe rendered case, taking a published optical model of the human eye into account. We compare our results to a model that conserves wavefront curvature. We then demonstrate how to optimize hogel sampling parameters as a function of image depth, size, and viewer distance. We conclude that stereograms suffer from little degradation from a viewing distance larger than 2 meters, but that nearer field images can significantly benefit by adding a second order phase correction.

1. Introduction

There historically have been two approaches for the rendition of holographic images, whether for real-life scenes or synthetic images. In the conventional method an entire scene is phase-encoded on the recording medium, either through interference from an actual object wavefront or by computation of the corresponding fringes. An alternative approach is to capture or calculate a number of discrete perspectives, which are then multiplexed after proper processing[1]. This stereographic approach makes it much easier to capture real life scenes using a conventional camera, is computationally less intensive in the case of synthetic images, and is commercially available. However, previous work on 2-step stereograms has demonstrated that discarding the second order phase information results in a loss of resolution in the case of deep images[2].

The goal of the current paper is to extend the modulation transfer function (MTF) analysis of references[2] and [3] to the case of 1-step hogel-based displays, some of which we have built at the College of Optical Sciences. These so called 1-step stereograms currently have largely supplanted the 2-step master / copy process pioneered by DeBitetto[4] and Benton[5] since they directly generate an in-plane hologram. The additional computational cost of the 1 step technique is no longer prohibitive for full parallax images and the technology has been deployed commercially.

2. 1-step image plane stereograms.

In the case of 1-step stereograms (sometimes referred as hogel-based stereograms), the direction of rays coming from a scene is discretely encoded within each individual picture element[1]. Each picture element, called a hogel, is printed separately in the geometry shown in Fig. 1. Although the stereogram is encoded interferometrically with a reference beam, the process does not conserve the 2nd order phase information (wavefront curvature) of the original scene. Instead, the wavefront curvature is approximated piecewise from the diversity of rays coming from a collection of hogels.

This loss of wavefront curvature leads to a decreased resolution in stereograms for picture elements away from the image plane, and also to aliasing artifacts if the image is improperly processed. A depth-dependent filter can be implemented to remove the artifacts. However, the loss of resolution can only be alleviated by encoding the wavefront curvature. Holographic stereograms that encode the second-order curvature information have been published by Bove's group at MIT[6]. They have been experimentally demonstrated to yield better images at a reasonable additional computational cost by using a look up table for the wavefront curvature. The principal inconvenient of the technique is that it places considerably more constraints of the spatial light modulator (SLM), which in that case has to be used as a phase modulator. With SLM's increases in performance and speed we will likely see more use of this method in coming years.

3. Wavefront errors in 1-step stereograms

In this analysis we will consider the wavefront description to be separable in X and Y axes, which is usually the case in practice due to the use of square and rectangular hogels and SLM pixels. We can then separately calculate the X and Y modulation transfer functions and express the system MTF by their product. It should be noted that our analysis does not account for astigmatism, which is a third order aberration. However, in the case of full parallax images, the astigmatic error is generally significantly smaller than wavefront curvature and can be ignored. In the case of horizontal parallax only (HPO) holograms the effect of astigmatism becomes more pronounced for deep images, but our model still provides a good approximation as we will see in the experimental section.

1-step holographic stereograms are well described in the literature so we will only succinctly describe the process in this article. The reader is referred to ref. for a more detailed explanation.

3.1. Recording

Fig. 1 gives a schematic representation of the recording of a single hogel for a transmission geometry. First, the scene of interest is calculated in a representation that corresponds to the 1-step recording geometry. This results in a 2x2 matrix representing the discrete vectors corresponding to the rays coming from the scene. Such a matrix is calculated for each hogel in the hologram. In the case of natural scenes, this process requires re-sampling the pixels corresponding to successive image perspectives in a process often referred to as *light field rendering*.

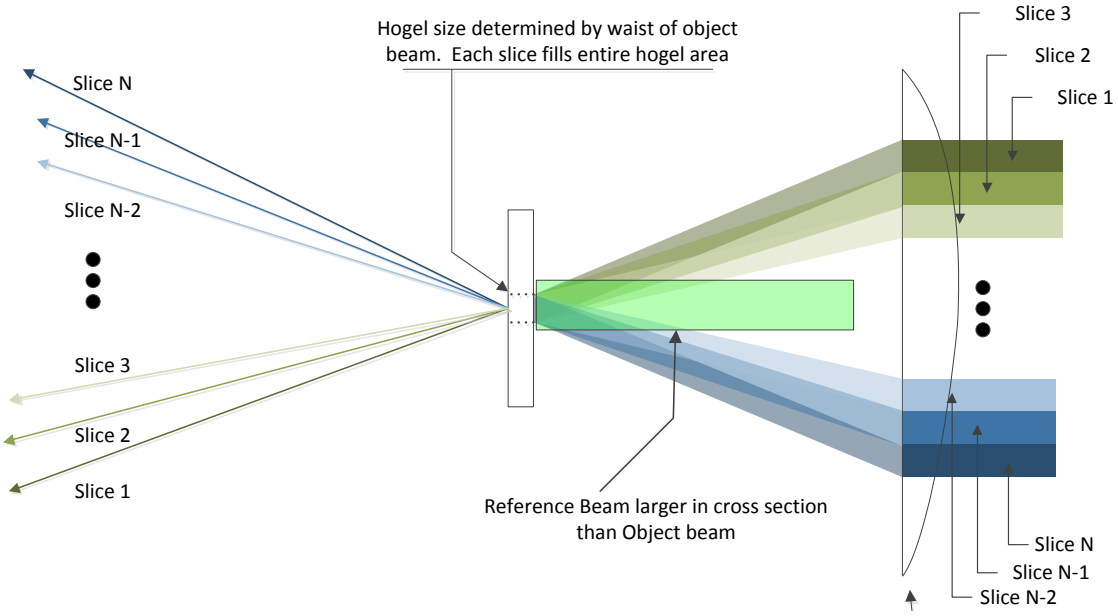

Figure 1. Hogel recording geometry.

After rendering, the matrix elements corresponding to the intensity of individual rays for a hogel are transferred onto the SLM as grayscale values, and the hogel is projected onto the recording medium where it interferes with a reference beam. Usually, the SLM is situated close to the Fourier plane of the objective lens, so that its conjugate image upon reconstruction lies in the far field. The view zone of the hologram will then be determined by the f/number of the objective lens, often requiring the use of custom made low f/number optics.

In practical systems the SLM is often relay-imaged onto the front focal plane of lens L1 where a diffuser is added to generate square uniform pixels. The effect of such a diffuser is not considered in the present paper. The effect of the diffuser is to spread the intensity of the ray bundle at the hogel plane in order to exploit the complete dynamic range of the medium, at the cost of a small decrease in resolution for deep images.

3.2. Reconstruction

The usual reconstruction consists in illuminating the stereogram with a conjugate of the reference beam, although a non-conjugate illumination can also be used (which is the case in our work at UA)[7]. Each ray direction (k-vector) then matches the recording geometry, but the radius of curvature is fixed by the focal length of the recording lens.

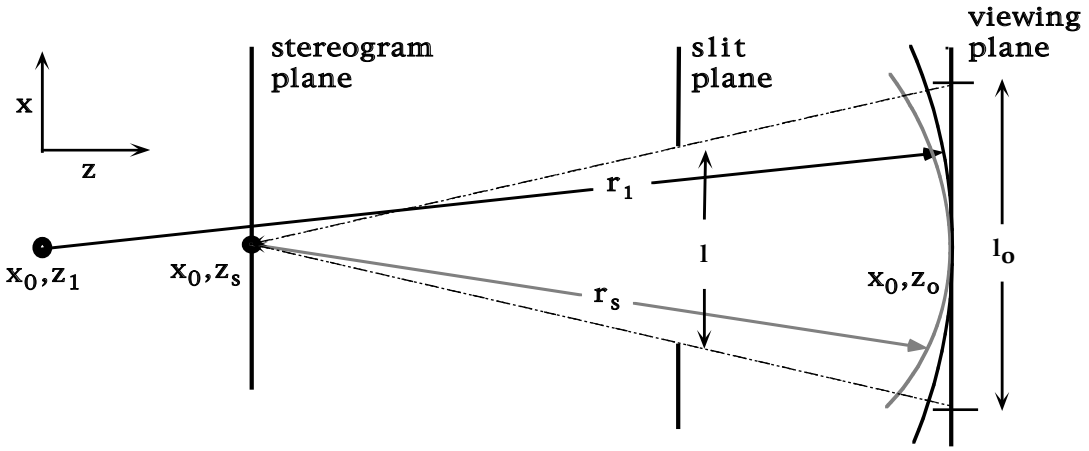

Figure 2. Wavefront curvature error. In the 1-step process the slit plane coincides with the objective lens position in Fig. 1, and l represents the extent of a SLM pixel.

The 1-step recording process thus creates errors during reconstruction because of this wavefront curvature mismatch. This discrepancy, which is not present in conventional holograms, is equivalent to a defocusing of the scene components away from the stereogram plane. The image degradation resulting from defocusing is well known and can be characterized by its effect on the modulation transfer function[8]. Such an analysis was previously applied to the analysis of conventional 2-step stereograms and Ultragrams (a generalization of the 2-step geometry for arbitrary slit position)[3]. Extending the results to the 1-step case is straightforward if we refer to Fig. 2.

The wavefront curvature error between the stereogram plane and the original object when measured at the viewer plane has the expression[3]:

$$\Delta r \approx \left(z_1 - z_s\right) + \frac{\left(z_s - z_1\right)}{2\left(z_1 + z_o\right)\left(z_s - z_o\right)}\left(x - x_0\right)^2 \tag{1}$$

And the real part of the pupil function as calculated from the viewer location is determined by the projection of each ray onto the viewer plane:

$$P(x) = rect\left[\frac{(x - x_0)z_s}{l(z_s - z_o)}\right] \tag{2}$$

where l is the spatial extent of a single perspective at the SLM plane. Note the sign convention: since we chose the origin to be at the Fourier transform lens plane, z1 and zs are generally *negative*.

Evaluating the optical transfer function (OTF) integral in an identical treatment to that of ref.[8] then leads to the result:

$$H\left(f_x^s\right) = \Lambda\left(\frac{\lambda\left|z_s f_x^s\right|}{l}\right)\mathrm{sinc}\left[\frac{(z_s - z_1)(z_s - z_o)l}{z_s(z_1 - z_o)} f_x^s\left(1 - \frac{\lambda\left|z_s f_x^s\right|}{l}\right)\right] \tag{3}$$

where the sinc function is defined as sinc(x) = sin(πx) / πx and the triangle function L is defined as:

$$\Lambda(x) = \begin{cases} 1 - |x| & |x| \le 1 \\ 0 & \text{otherwise} \end{cases} \tag{4}$$

The modulus $|H|$ of the OTF is referred as the modulation transfer function and is an important measure of image quality in optical systems.

Equation (3) can be more conveniently be expressed in terms of the image depth D, SLM size S (or its image at the objective Fourier plane if relay optics are used), number of perspectives N, and observer position Z_0 with respect to the hologram plane as:

$$H\left(f_x^s, D\right) = \Lambda\left(\frac{\lambda N\left|z_s f_x^s\right|}{S}\right)\mathrm{sinc}\left[\frac{D z_o}{z_s(D - z_o)}\frac{S}{N} f_x^s\left(1 - \frac{\lambda\left|z_s f_x^s\right| N}{S}\right)\right] \tag{5}$$

where z_s now denotes the focal length of the objective lens L_1. In equation (5) we have adopted the convention that D is positive in front of the hologram for non-conjugate illumination, and negative for conjugate illumination, while the viewer position z_o is always positive. The maximum spatial frequency in the reconstruction is bounded by:

$$f_x^{s\max} = 1/2H \tag{6}$$

where H is the size of a single hogel.

As an example, let us consider an image that straddles the hologram plane and has a depth ranging from 20 cm in front of the hologram to 20 cm behind with a hogel size of 0.25 mm and view zone of 30 degrees. What would be the MTF vs. depth of the image for a viewer 0.8 m away with 100 and 250 rendered individual perspectives (or equivalently number of angular samples per hogel)?

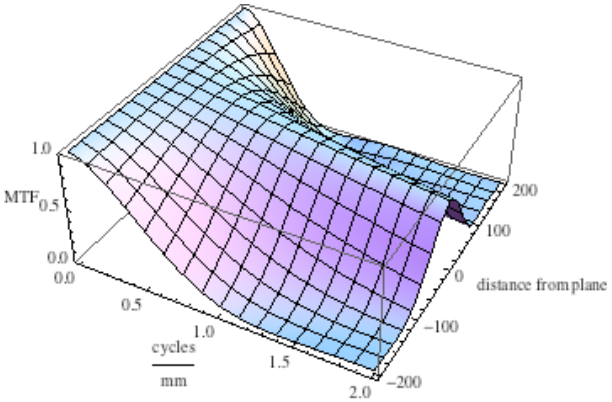

Figure 3. MTF vs. depth (100 views).

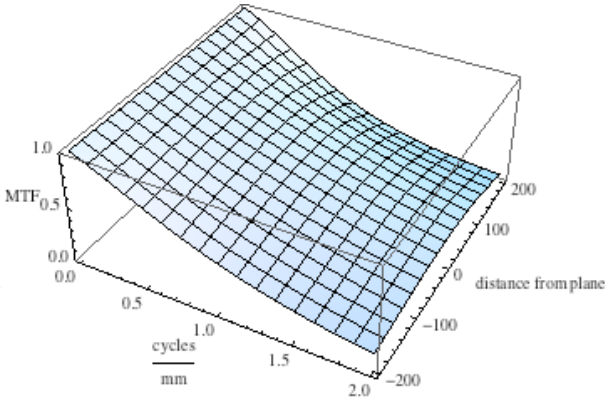

Figure 4. MTF vs. depth (250 views).

As we can see, increasing the number of perspective to 250 results in a much sharper image away from the plane of the hologram at the expense of a loss of contrast closer to the plane.

It is interesting to compute the image sharpness at maximum depth versus the number of perspectives N. We get the following curves for depths of 50, 100, and 200 mm for a spatial frequency of 2 cycles/mm.

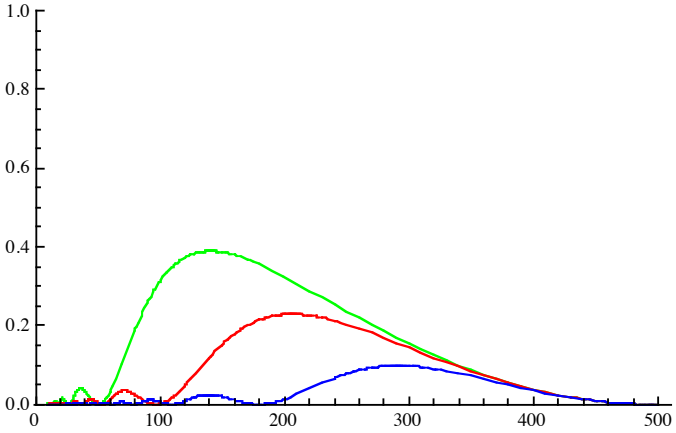

Figure 5. MTF curves for depths or 50, 100, and 200 mm *vs*. number of perspectives.

Clearly more perspectives result in a higher image resolution for deep images, and the number of perspective views should be chosen to match the depth of the reconstructed image and size of the hogels.

For an ideal optical hologram, the equivalent MTF would have an almost constant value close to 1, demonstrating that the preservation of local phase has a profound effect on hologram reconstruction. However we are now led to ask how much this matters for the perception of the image by the observer's visual system. Answering this question requires a physical optics model of human visual perception.

4. Human visual system MTF

It is essential to consider the response of the visual system when comparing different modalities of hologram recording such as phase vs. non-phase conserving displays. In this section we will use a model of the human eye MTF derived by Artal and Navarro, who used a double pass system to directly measure the contrast of images projected onto the retina[9]. The measurements were then

fitted to an empirical double exponential curve. We will summarize the salient point of this description as following:

- The human eye is not diffraction limited. Only for a pupil size of 1.5 mm or less does it approximates a diffraction-limited system.
- Acuity goes down as pupil increases in size (up to 8 mm), so display brightness affects performance. Brighter displays look crisper.
- The numerical models of the eye MTF that have been published do not completely agree, but their differences are minor with respect to this work.
- Higher order aberrations extend the depth of field for larger pupil sizes, a natural example of wavefront coding.

It should be noted that here is a difference between the objective eye MTF (contrast measured on the retina by an ophtalmoscope, such as in our model), and the subjectively perceived MTF (also called "neural" MTF), which includes cognition and neural processing and is determined by psychophysical measurements. Using the retinal MTF as we do generally puts stricter requirements on the display, since the human visual system is good at "filling out" details. However it fits better this analysis, which is all based on physical optics.

As an example, figure 6 shows the object space MTF for a viewer 800 mm away for pupil sizes of 2.5 and 7 mm.

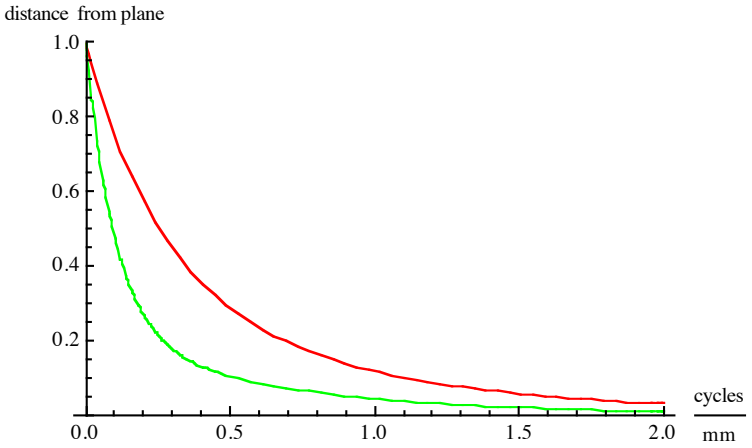

Figure 6. Modeled eye MTF for pupil diameters of 2.5 (red), and 7 mm(green).

Having obtained numerical models for both the display and visual system, we can now calculate the MTF of the optical system comprising both the display and human eye with the formula:

$$MTF_{system}\left(f_x^s, D\right) = MTF_{display}\left(f_x^s, D\right) \times MTF_{eye}\left(f_x^s, D\right) \tag{7}$$

In which MTF_{system} is given by equation 5 and MTF_{eye} corresponds to the numerical approximation of ref. [9]

For the rest of this article we assume a viewer pupil size of 2.5 mm, which is a realistic value when working with information displays. If we now plot MTF_{system} with the same parameters used in fig. 4 and 6, we get the following plots for a hogel-rendered display and a curvature preserving display:

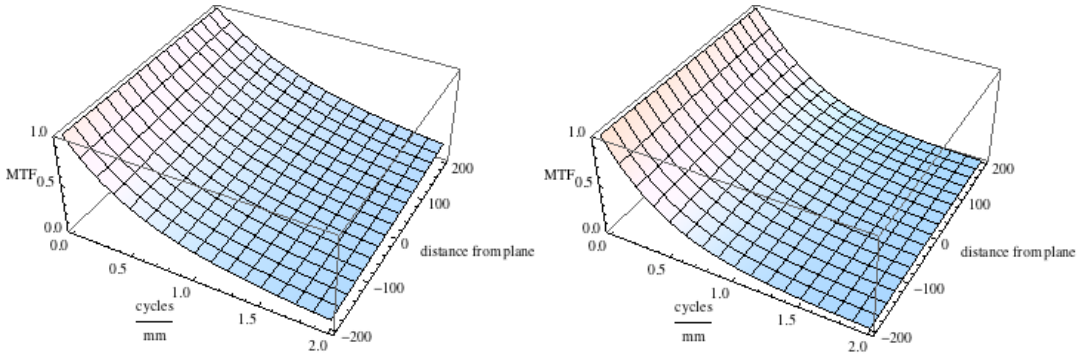

Figure 7. System MTF that includes the observer visual system using (left) full fringe rendering. (Right) Hogel based rendering. Eye pupil size is 2.5 mm.

As we can see, the limited MTF of the human eye considerably levels the playing field between phases preserving displays and hogel-based displays, although there is still is a noticeable difference.

The last parameter we have yet to explore concerns the viewer position with respect to the hologram plane. As an example, lets consider the case of observer positions 500, 800, and 2000 mm away. We get the following curves for reconstruction 200 mm in front of the hologram:

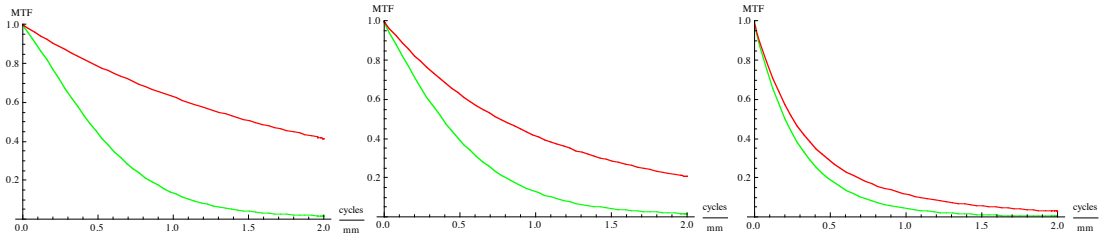

Figure 8. System MTF for a viewer distance of (right) 500, (center) 800, and (left) 2000 mm. The fringe-rendered MTF is in red and the hogel based MTF in green. Eye pupil size is 2.5 mm.

Fig. 8 illustrates how for deep images the hogel-based reconstruction dramatically degrades with respect to a coherently-rendered image as the viewer closes in to the reconstruction.

5. Discussion

The model was implemented in *mathlab* and *mathematica*, and was used to simulate the displays that our group built at the College of Optical Sciences. Having a working model allowed us to optimize both the computation and the optics of our systems, by comparing the experimental measurements to the numerical predictions. As a result, we were eventually able to write images in our photorefractive polymer that approximated the modeled MTF to within 30%, despite using off the shelf optical components (with the exception of the holographic diffusers that were fabricated in-house). As an example, figure displays the Air Force test chart written on our material at the focal plane and 90 mm in front. In this case the hogels had a 250 micrometer extent and 200 views were rendered for a total viewing angle of 26 degrees. Getting close to the predicted performance took a considerable amount of effort. Besides the design and careful alignment of optics, we had to fabricate our own LED illuminators and volume holographic band-limited diffusers. A more detailed description of our experimental work is also published these proceedings.

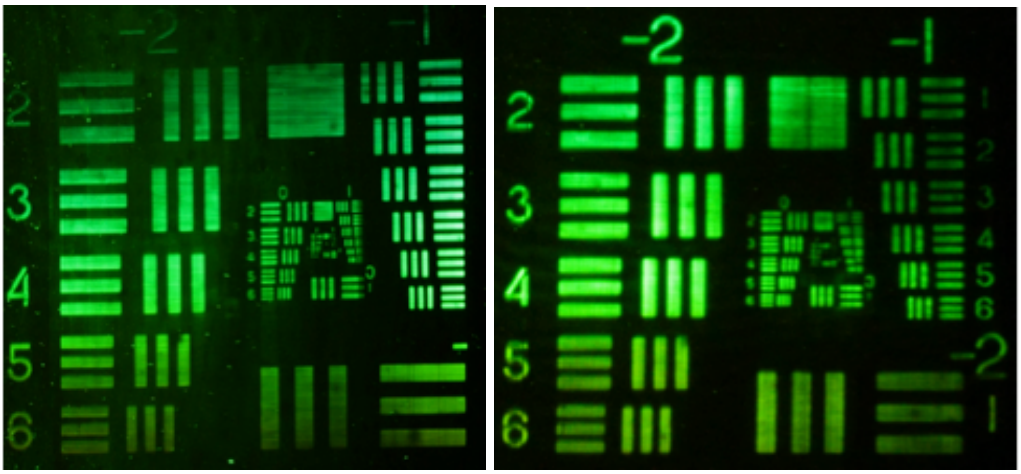

Figure 9. Air force test chart imaged (a) at the hologram plane and (b) 90 mm in front. 100 views were calculated over a total view zone of 26 degrees. Individual hogels have a 250 micron extent.

6. Conclusion

Are holographic stereograms truly holograms? We answer the question by saying that it is all in the position of the beholder. For situations equivalent to working on a desktop display or tablet computer, or for displaying medical data such as CAT scans or MRIs, the functionality of stereograms might be hampered because their resolution is reduced for deep images, despite their accurate rendition of occlusion and stereopsis depth cues. In other situations, such as televisions, advertising signage, or computer augmented virtual environments (CAVEs), the difference is hardly meaningful and the word "hologram" can be legitimately used. This is an old debate and this article does not expect to have the last word. However, from our simulations, practical holographic workstations for CAD/CAM or medical imaging will likely require wavefront curvature preservation. It also became clear within the scope of this work that light source engineering (including the use of resonant or photonic lattice LED's) is an essential element in these novel imaging systems.

We acknowledge support from AFOSR, DARPA and the NSF ERC Center on Integrated Access Networks (CIAN).

7. References

[1] S.A. Benton and M. Bove, "*holographic Imaging*", J. Wiley ed. (2011).
[2] Pierre St Hilaire, "Modulation transfer function and optimum sampling of holographic stereograms", Applied Optics, Vol. 33, No 5, Feb 1994, pp. 768-774.
[3] P. St. Hilaire, "Optimum sampling parameters for generalized holographic stereograms", SPIE Proceedings #3011 "Practical Holography XI". S.A Benton editor, pp. 96-104.
[4] D. J. De Bitetto, "Holographic Panoramic Stereograms Synthesized from White Light Recordings," Applied Optics, Vol. 8-8, pp. 1740-1741 (August 1969).
[5] S. A. Benton. "Achromatic Holographic Stereograms", J. Opt. Soc. Amer. , Vol. 71-12. p 1568A (December 1981).
[6] Q. Y. J. Smithwick, J. Barabas, D. E. Smalley, and V. M. Bove, Jr., "Interactive Holographic Stereograms with Accommodation Cues," *Proc. SPIE Practical Holography XXIV,* v. 7619, 2010.
[7] S. Tay *et al*. "An updatable holographic three-dimensional display", *Nature* 451, 694-698 (2008).
[8] J. W. Goodman, "Introduction to Fourier Optics", (Mc Graw Hill Book Co., San Francisco, 1968), pp. 101-133.
[9] P. Artal and R. Navarro, J. Opt. Soc. Am. A, Vol. 11, No. 1, 1994.